Heriot-Watt University

Heriot-Watt University
Research Gateway

Heat transfer enhancement to a confined impinging synthetic air jet

Rylatt, Daniel; O'Donovan, Tadhg

Link to publication in Heriot-Watt Research Gateway

Heat Transfer Enhancement to a Confined Impinging Synthetic Air Jet

D. I. Rylatt* and Tadhg S. O'Donovan

School of Engineering and Physical Sciences, Heriot-Watt University
*Corresponding Author E-mail: dir1@hw.ac.uk

ABSTRACT

Heat transfer to confined, un-ducted and ducted impinging synthetic air jets is investigated experimentally. The influence of ducting on the cooling performance of synthetic air jets is of particular interest. Heat transfer to the jets is reported for a range of experimental parameters including jet exit to impingement surface spacings, H/D (from *0.5* to *3)*, ducting outlet diameter (*1.2*, *1.6* and *2* jet diameters) and length of the confining plate (*90 to 200mm*). It is shown that increasing the length of the confining plate reduces the cooling performance by up to 14% in the stagnation region and 8% on an area averaged basis. Ducting is added to the jet to improve heat transfer by drawing cold air from a remote location into the jet flow. Across the range of parameters tested, ducting offers the largest increase in heat transfer at *H/D=1*; at this spacing the *2* jet diameter ducting outperforms all others and can increase the heat transferred to the jet in the stagnation region by 27% and by *36%* on an area average basis. At nozzle to impingement surface spacings greater *1* diameter ducting with a *1.6* jet diameters outlet offers the largest increase in heat transfer.

KEYWORDS

Synthetic jets, thermography, ducting, confinement, convection

1 INTRODUCTION

Jet impingent heat transfer has, for many years, been used in industry for applications such as the cooling of turbine blades[1], manufacturing processes such as grinding [2] and the thermal management of electronics [3]. This is due to the high localised and area averaged heat transfer coefficients jet impingement can achieve. Synthetic air jets are a promising new technology which has been shown by both Smith and Swift [4] and Pavlova and Amitay [5] to be capable of providing more than twice the cooling of continuous air jet impingement for a similar range of Reynolds numbers.

The processing power of computers has increased greatly in recent years leading to higher demands placed on thermal management systems. This increase in processing power has been accompanied by a steady reduction in size and the available space in computers due to the desire for increased functionality in the same or smaller housing. Kercher et al. [6] have shown that a synthetic air jet using the same power as a standard commercial fan can provide more than twice the cooling. Saini and Webb [7] have shown the heat rejection limit of a fan/fin heat exchanger, currently employed in computers, to be approximately 100W. The current CPU Thermal Design Power (TDP) for an Intel® Core™ i7-860 is 95W and the TDP of the Pentium 3 circa 1999 was around 35W. While this shows that Gunther's [8] prediction in 2001 of a twofold growth in the TDP every two years was not realised, it is clear that the fan-fin heat exchangers will not meet the growing cooling requirement of electronic component. New technologies, such as synthetic air jets have the potential to meet this requirement.

A synthetic jet is a time averaged fluid motion which is formed by the periodic oscillation of a diaphragm bounded to a cavity containing an orifice. The periodicity and amplitude of the oscillatory flow dictate whether or not a jet is formed. Holman et al [9] have shown the formation criteria to be strongly dependent on the Strouhal Number ($Str^{-1}=Re/St^2 > K$) where the constant, K is dependent on geometric factors such as orifice shape, radius of curvature and aspect ratio. Synthetic jets are characterised using two dimensionless parameters, Reynolds number and stroke length. The velocity scale used in these parameters is suggested by Smith and Glezer [10] to be the downstream directed velocity on the expulsion stroke of the jet cycle. Persoons and O'Donovan [11] have shown that by measuring the pressure in the jet cavity, the exit velocity of the jet can be calculated using conservation of momentum at the jet orifice. Synthetic air jets are compact and require no external plumbing which makes them an attractive technology for space restricted applications such as electronics cooling. Synthetic air jet technology has not been implemented in electronics cooling applications due to their relatively poor performance in confined conditions; the current research addresses this limitation.

Chaudhari et al [12] have shown that a synthetic jet has a maximum heat transfer performance at a nozzle to impingement surface spacing of 10 jet diameters ($H/D=10$). At a nozzle to impingement surface spacing of *3* diameters however this is reduced by *80%*. Persoons et al [13] present heat transfer data for an axisymmetric jet similar to that used in this study; they found a reduction in cooling efficacy when the jet operates below its optimal spacing of 3.4 jet diameters. Smith and Glezer [10] and Smith and Swift [4] compared the heat transfer performance of synthetic and steady impinging air jets. They have shown that the high rates of heat transfer achieved by synthetic jets are attributable to the high rates of growth in both the jet column width and volume flux due to entrainment when compared to steady jets. This is limited at lower nozzle to impingement surface spacings.

Further to this, at low *H/D*, the fluid between the heated impingement surface and the jet orifice plate is highly confined and is therefore re-circulated in the jet flow. The fluid is at an elevated temperature above that of the surrounding ambient air and is drawn into the jet on the suction stroke of the jet and then expelled towards the heated surface. The reduced temperature difference between the synthetic air jet and the impingement surface therefore results in substantially reducing cooling performance.

Numerous studies have investigating the effects of confinement on the heat transfer to steady impinging jets [14-18]. Youn et al [18] investigated the effects of confinement of a microscale steady jet for a wide range of confining plate lengths, L_{op} (*3 to 48* jet diameters) and nozzle to impingement surface spacings, *H* (*1 to 20* jet diameters). Overall,

confinement is shown to reduce the heat transfer as the heated outflow is confined between the jet and the impingement surface. At low nozzle to impingement surface spacings, even relatively minor confinement ($L_{op}/D=6$) can reduce the stagnation point heat transfer by more than 50%. In general, at low H/D however, further increasing the confinement does not lead to substantial further reductions in the surface heat transfer, but it does however, affect the height at which the effect of the increased plate length will be overcome. Herein lies one significant difference between steady and synthetic air jet impingement heat transfer. Chaudhari et al [12] investigated the effect of increasing the confining plate length of a synthetic jet from L_{op}/D = *7.86* to *13.75*. Heat transfer to the more confined impinging jet was less than *50%* of the heat transfer to the less confined jet for the range of nozzle to impingement surface spacings tested (*H/D=1 to 14*). Therefore, it is clear that heat transfer to confined impinging synthetic jets is significantly different from steady jets, which only display the effects of increased confinement at low H/D.

Pavlova and Amitay [5] and Persoons and O'Donovan[19] have presented measurements of an impinging synthetic air jet velocity flow field using particle image velocimetry. It is apparent from the results presented that fluid is entrained from the sides and parallel to the orifice plate during the intake stroke. The jet flow formed by the expulsion stroke is therefore normal to the intake fluid. This research has taken advantage of these orthogonal flow streams; by introducing ducting parallel to the orifice plate, the confined jet flow is separated from the intake stream. Thus, without using valves which would increase the pressure drop and hence power requirement, a passive method of enhancing the heat transfer to an impinging synthetic air jet is proposed.

Impinging synthetic jets can achieve higher rates of heat transfer than the current fan-fin configurations. Synthetic jets therefore have the potential to meet the growing thermal management need of the electronics industry. It is clear that if the limitation of synthetic jet in confined situations can be overcome they have the potential to be a viable alternative to existing cooling technology. The objective of the current experimental research therefore, is to develop a synthetic air jet that reduces the re-circulation of air at low nozzle to impingement surface spacings and negate the effects of confinement; this has been achieved by the addition of ducting parallel to the jet orifice plate.

2 EXPERIMENTAL FACILITY

A schematic of the experimental setup is presented in figure 1; the facility consists of two main components: 1) the synthetic air jet assembly, and 2) a heated impingement surface. The jet is mounted directly above the heated surface with the jet flow perpendicular to it. As can be seen in figure 1, the synthetic air jet consists of a cavity with an acoustic speaker operating as the jet diaphragm on one end, and the jet orifice opposite it. The cavity diameter is *76mm* and has a depth of *30mm* and the circular orifice is *5mm* in diameter and *10mm* long. All dimensions are accurate to within *0.1mm*. The synthetic jet actuator is a Visaton© FR8 *8Ω* acoustic speaker which is powered by a sinusoidal voltage signal generated by a Thurlby Thandar Instruments TG315, and amplified by a Kemo® MO 034 *40W* power amplifier. The jet assembly is attached to a Manfrotto 454 micro positioning plate to allow for fine adjustment of the distance between the synthetic air jet and the impingement surface. A GRAS 40PL microphone and a T-type thermocouple are embedded in the cavity of the jet to allow for cavity pressure and temperature measurement; these are recorded using National instruments DAQ NI9233 IEPE Dynamic Signal Acquisition module and a NI9211 thermocouple module and logged using LabVIEW.
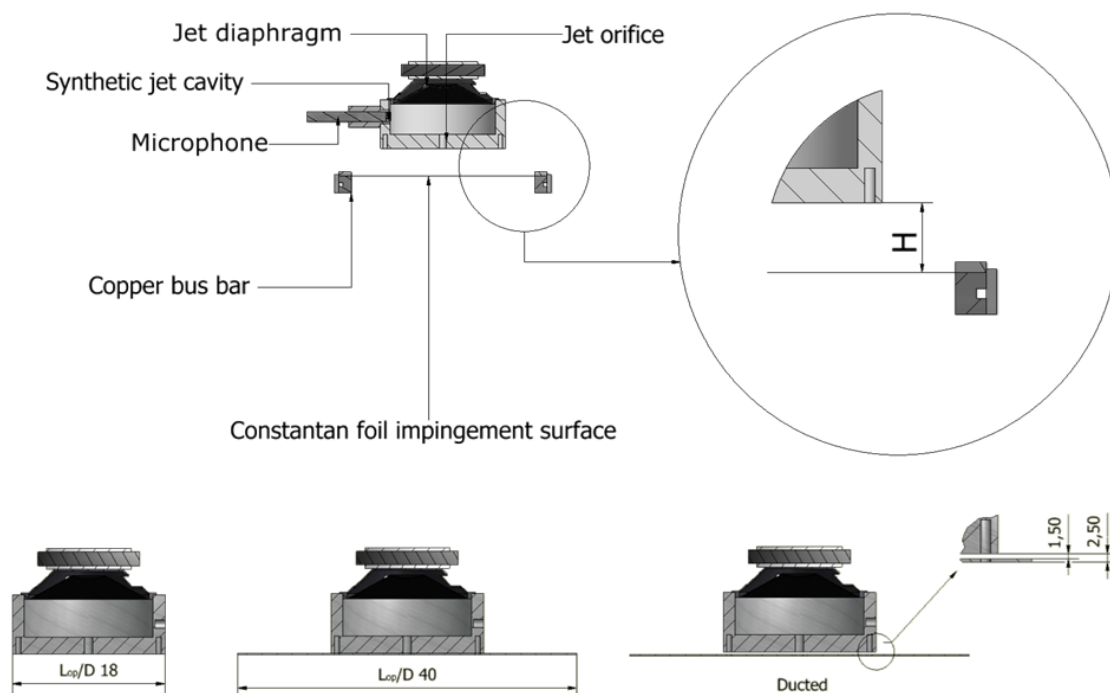

Figure 1: Schematic of the experimental setup and jet configurations

Ducting plates are fabricated from 1mm thick stainless steel laser cut to 200mm by 200mm with a tolerance of 0.01mm. Each ducting plate has a circular outlet located at the centre of the plate to allow the jet to flow through. In the current investigation three ducting plates are tested with hole diameters of *6, 8* and *10mm*. The plates are attached to the jet with a clearance of *1.5mm* from the jet exit. This distance was chosen so that a) the cylindrical area, through which the air is drawn into the jet cavity, is larger than the area of the orifice for all ducting configurations and b) jet orifice can be placed close to the impingement surface. A full parametric study on the ducting plate dimensions and positioning has yet to be conducted.

In this study, the cooling performance of a synthetic jet is evaluated for three test configurations, namely un-ducted, un-ducted with increased semi-confined and ducted. The impingement surface consists of a thin resistance heater foil that has a surface area of 150mm × 100mm and approximates a uniform wall flux thermal boundary condition. Constantan® Resistance Alloy (Cu55/Ni45) foils of thickness 10, 25 and 50μm were used in this research; the foils were provided by Goodfellows Cambridge Ltd. The undersides of the foils were lightly coated with a matt black paint to

4

increase the surface emissivity value to approximately 0.97; this was necessary to ensure accurate surface temperature measurements with an infrared thermal imaging camera. The foils are clamped between two copper bus bars. The bus bars are held in place by two electrically insulating nylon struts, one of which is attached to two linear bearings to allow for positioning and tensioning of the foils. A direct current voltage is applied across the foil via the bus bars by a Farnel AP *20 - 80* regulated power supply which is capable of supplying up to *80Amps*. To ensure minimum losses in transmission, a *35mm^2* cross sectional core copper welding cable was used to connect the bus bars to the power supply. All the components of the experimental setup are contained within a frame constructed of *45mm* by *45mm* extruded aluminium profile

A CEDIP Titanium 560 Indium Antimonide detector 3 – 5 μm waveband high speed thermal imaging camera is mounted directly beneath the heated surface. The camera is used to measure the surface temperature of the foil with high spatial and temporal resolution. The frame rate used in the current study is *400Hz* which yields an image of *640 x 64* pixels. The field measured by the camera at this resolution is *105 x 10.4mm* which corresponds to an image resolution of *30.7* pixels per jet diameter. The camera has a noise equivalent temperature difference (NETD) of <18*mK* at *30°C* and a range of *-20* to *3000°C* with an absolute temperature accuracy of *±1%*. The camera is also attached to a Manfrotto 454 micro positioning plate. For all tests the maximum operating temperature of the foils was less than *100°C*. Each dataset is *20* seconds in duration which result in *8000* individual images.

Heat transfer data are presented in the form of the time-average and time-varying Nusselt number distributions and use the diameter of the jet to normalise the surface convective heat transfer coefficient; this is calculated using equations 1 to 6.

$$q''_{gen} = \frac{VI}{A_{surf}} \tag{1}$$

$$h = \frac{q''_{gen}}{(T_{surf} - T_{jet})} \tag{2}$$

Equation 2 is based on the assumption that heat generated within the foil is conducted in 1 dimension through the thickness of the foil before convecting to the impinging jet. Patil and Narayanan [20] also investigated the application of the thin foil infrared thermography technique for heat transfer measurements in convective flows and found that "lateral conduction heat flux rate contributed a significant portion to the net heat entering the control volume". Therefore, in order to accurately assess the local heat transfer taking place from the foil to the impinging jet, lateral conduction must be considered. A correction for lateral conduction similar to the one used by Golobic et al [21] and shown in equation 3 was used in this study to calculate the mean and time-varying surface heat transfer coefficient.

$$h = \left\{ \frac{q''_{gen} + \delta k \left(\frac{\partial^2 T_N}{\partial x^2} + \frac{\partial^2 T_N}{\partial y^2} \right)}{T_N - T_\infty} \right\} \tag{3}$$

Where

$$\frac{\partial^2 T_N}{\partial x^2} = \frac{T_{X+1,N} + T_{X-1,N} - 2T_{X,N}}{\Delta x^2} \text{, etc} \tag{4}$$

$$Nu = \frac{hD}{k} \tag{5}$$

Figure 2 shows the uncorrected heat transfer distributions calculated using equation 2 for three foil thicknesses. Figure 3 shows the same data once the correction technique shown in equation 3 has been applied. Once lateral conduction has been taken into accounted all three heat transfer distributions converge, confirming the validity of the correction technique.
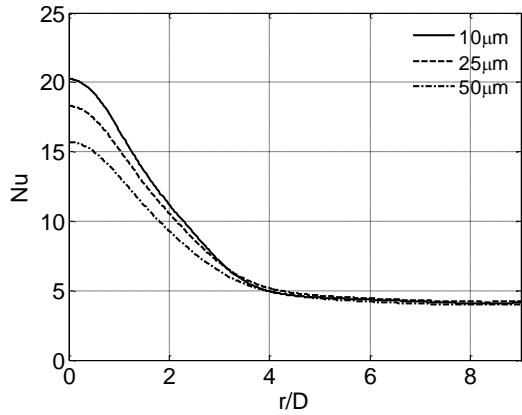

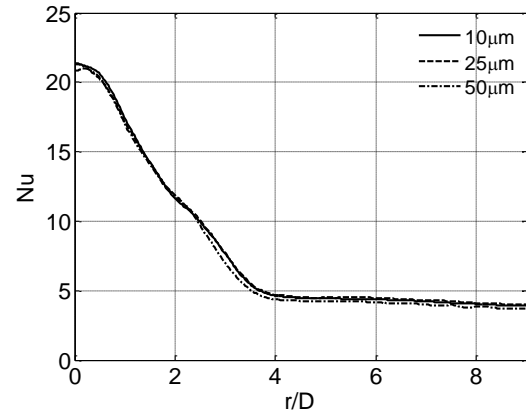Figure 2: Uncorrected Nusselt number profiles

Figure 3: Corrected Nusselt number profiles

A synthetic jet is defined primarily by two dimensionless parameters, the Reynolds number and stroke length. The stroke length, L_0 is defined by Smith and Glezer [10] as the integral of the jet exit velocity, u_0 with time for the expulsion stroke:

$$L_o = \int_0^{\tau/2} u_0(t)dt \tag{6}$$

where τ is the period of the cycle. The velocity used to calculate the jet Reynolds number, Re is based on this stroke length:

$$U_0 = \frac{L_0}{\tau} \tag{7}$$

Hence the synthetic jet Reynolds number, Re, may be calculated as in equation 9:

$$Re = \frac{U_0 D}{\nu} \tag{8}$$

In this investigation the jet outlet velocity is not measured directly but rather the time varying relative pressure of the cavity is measured and the jet exit velocity calculated via the method proposed by Persoons and O'Donovan [11]. By using the conservation of momentum in the orifice the time varying jet exit velocity can be calculated as follows:

$$m\frac{dU}{dt} + F_D(U_0) = pA \tag{9}$$

Where $F_D(U_0)$ represents a damping force, and $m = \rho A L'$ is the mass of gas in the orifice. The effective length L is the sum of the geometric length L and end corrections $L'−L=2ßD$; $ß=0.425$ [22] for a sharp-edged circular orifice.

The uncertainty in the Nusselt number is calculated to be less than 3% for a fixed Reynolds number of 3000 and stroke length of 15 which have uncertainties of 3.5%.

3 RESULTS

In order to make the heat transfer performance of the jet relevant to the task of electronics cooling a jet was selected which offers similar heat transfer rates to that of a commercially available CPU cooler. One such cooler was tested by Kercher et al [6] and was shown to be able to produce a heat transfer coefficient in excess of $400W/m^2K$ when used in conjunction with a finned heat exchange surface. When the fan was accessed cooling a flat heated surface *50.8* by *50.8mm* the convective heat transfer coefficient was $44W/m^2K$. The jet used in this investigation was generated using a constant excitation frequency of *65Hz;* the Reynolds number is set at *3000* which has a corresponding dimensionless stroke length, L_0/D, of *15*. The results presented in this section show that equivalent rates of heat transfer are produced by this jet.

Mean and RMS heat transfer distributions extending radially beyond 8 jet diameters to impinging synthetic air jets are presented in this section. Profiles of the magnitude of the Nusselt number fluctuations are presented to give some insight into the level of turbulence in the flow next to the wall. The surface heat transfer is also compared on an area averaged basis for the stagnation region and for an area equivalent to a CPU heat sink. This is done for un-ducted, confined and ducted impinging synthetic air jet impingement configurations

3.1 HEAT TRANSFER DISTRIBUTIONS FOR SYNTHETIC AIR JET IMPINGEMENT

Time averaged heat transfer distributions are presented in figure 4 for a range of nozzle to impingement surface spacings where the synthetic air jet is unconfined, other than by its own geometric size. For the full range of nozzle to impingement surface spacings tested heat transfer is a maximum in the stagnation region and decreases with increasing radial distance. It is noticeable that heat transferred at the stagnation region of the jet is relatively constant (within 8% of the maximum value at *H/D=1.5*) over the range of jet spacings tested. There is a tendency towards lower rates of heat transfer for higher values of *H/D*; this is attributed to the jet spreading more before impingement resulting is slightly lower arrival velocities. Figure 5 shows the RMS of the heat transfer for the same range of test parameters. Unlike the heat transfer, there is a significant change in the magnitude of the fluctuations in the heat transfer for the full range of *H/D*, especially in the stagnation region. As *H/D* increases the arriving jet is more turbulent; it has been shown by Gardon and Akfirat [23] for steady jet impingement heat transfer that increased turbulence results in higher rates of heat transfer. The fact that these higher levels of turbulence serve only to maintain the rate of heat transfer to the jet at the same level with increasing *H/D* suggest that other effects are competing to lower the stagnation region heat transfer. At lower jet spacings the presence of the orifice plate confines the flow between the orifice plat itself and the impingement surface. This, in turn reduces the amount of ambient cold air entrained in the jet flow and increases the amount of re-circulated heated air, and therefore acts to reduce the magnitude of the surface heat transfer.
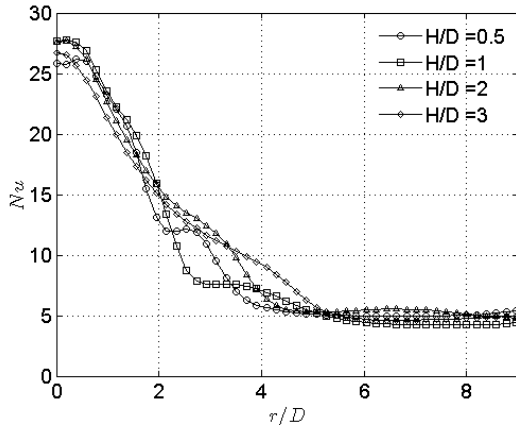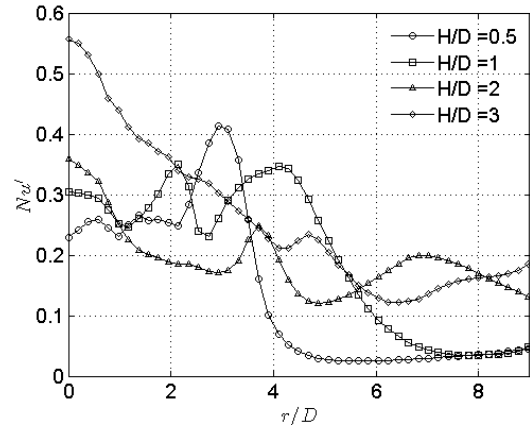
Figure 4: Nusselt Number Distributions; *Re=3000, L₀/D=15*

Figure 5: Fluctuating Nusselt Number Distributions; *Re=3000, L₀/D=15*

3.2 EFFECT OF INCREASED CONFINEMENT ON HEAT TRANSFER RATE OF A SYNTHETIC AIR JET

To assess the effect of increased confinement on the surface heat transfer to a synthetic jet, a plate is attached to the bottom of the jet which had an orifice of diameter *1 D*. This increases the length of the orifice plate from $L_{op}/D=18$ to *40* as is can be seen in figure 1.A study by Youn et al [18] have proposed a correlation for stagnation Nusselt number for a steady impinging jet as a function of *Re*, L_{op}/D and *H/D*. figure 6 shows the results of a comparison between the current study and the correlation presented by Youn et al [18] for a jet with a Reynolds number of *3000* and confined to *lop/D =18*, as can be seen the synthetic jet outperforms the steady jet by a factor of three across the range of jet to impingement surface spacings tested.
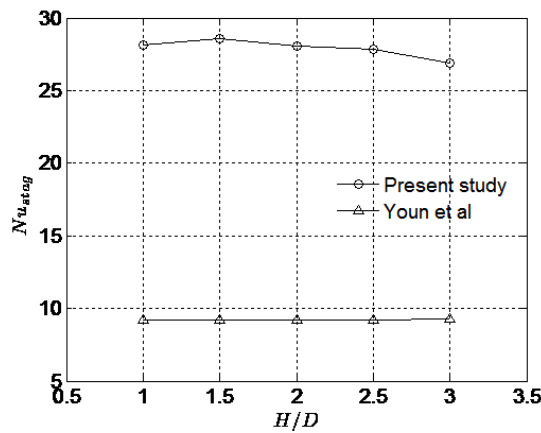

Figure 6: comparison of results with stagnation Nusselt number correlation
presented by Youn et al [18], $L_{op}/D=18$, *Re=3000*

Figure 7 shows the stagnation region Nusselt number h_{stag} for jet to impingement surface spacings from *0.5* to *3D* for two configurations, with and without the confinement plate. h_{stag} is the local heat transfer averaged over a circular area extending 1 diameter from the geometric centre of the impinging jet. This area was selected to give an indication of the maximum heat transfer available from the jet for task cooling application. The stagnation region heat transfer for the relatively unconfined case ($L_{op}/D=18$) is shown in figure 7 to be low seen that h_{stag} at *H/D=0.5*; this is attributed to confinement at such low nozzle to impingement surface spacings. As *H/D* increases, so too does the heat transfer as ambient air is entrained in the jet flow. The maximum stagnation region heat transfer is achieved at *H/D=1.5*; this is a *7.5%* increase even though the arrival velocity of the jet is likely to be lower at this spacing. At spacings greater *H/D=1.5*, the heat transfer decreases with further increases in *H/D*.
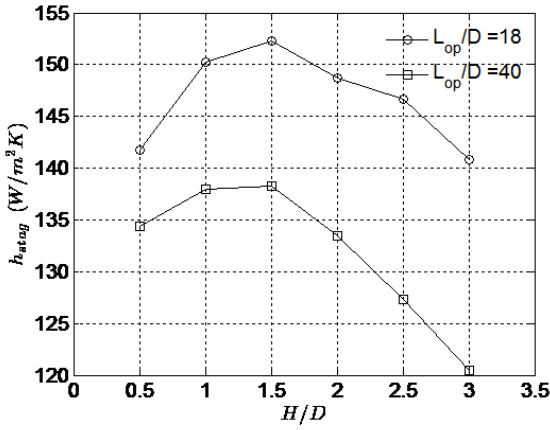
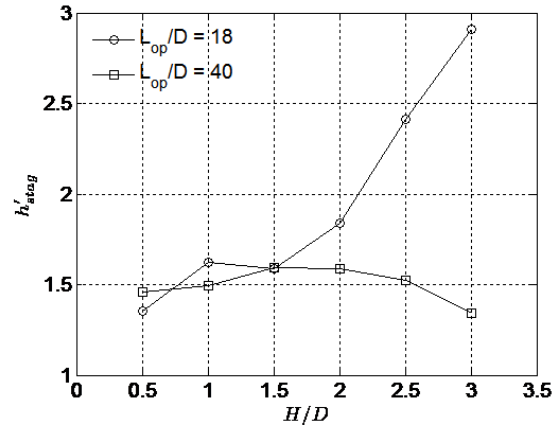Figure 7: h_{stag} for semi-confined jet at *Re=3000* $L_0/D=15$

Figure 8: h'_{stag} for semi-confined jets *Re=3000* $L_0/D=15$

By comparing the graphs for $L_{op}/D=18$ and $L_{op}/D=40$ it is clear that increasing the length of the orifice plate has reduced the magnitude of heat transferred to the jet in the stagnation region across the full range of *H/D* tested. It is also evident that both configurations reached their maximum h_{stag} at *H/D=1.5*. At larger jet to impingements surface spacings, the heat transfer to the $L_{op}/D=40$ jet reduced more significantly than for $L_{op}/D=18$.

The magnitude of the stagnation region heat transfer fluctuations for a similar range of parameters is presented in figure 8. It can be seen that the level of fluctuations remain similar for *H/D≤1.5*; at larger spacings the trends diverge and at *H/D=3* the fluctuations in heat transfer for $L_{op}/D=18$ are double those of $L_{op}/D=40$. It is therefore evident that the more rapid decline in the heat transfer to the $L_{op}/D=40$ jet at *H/D≥1.5* seen in figure 7 is due to the increase in orifice plate length reducing the turbulence in the impinging synthetic air jet flow.

Figure 9 shows the area averaged heat transfer ($\bar{h}$) for jet to impingement surface spacings from *0.5* to *3D* for the two confinement configurations. $\bar{h}$ is the heat transfer averaged over a circular area extending to a distance of *7D* from the centre of impingent; this area is selected because it is comparable with the size of commonly used CPU heat exchangers [7]. Also, within this range, secondary peaks in heat transfer distribution occur (figure 4) and will contribute to the overall cooling capacity of the technology.

The area averaged heat transfer of the low confinement jet ($L_{op}/D=18$) in figure 9 is low at *H/D=0.5* and *1*. The decrease observable from *H/D=0.5* to *H/D=1* is due to the level of heat transfer achieved by the jet at *r/D>5*. It can be seen in figure 4 for *H/D=1* that for *r/D>5* the heat transfer to the jet falls to a lower level than at *H/D=0.5*. It is worth noting that while the peaks in heat transfer at *H/D=0.5,* observable in figure 4, at *r/D=3* are higher in magnitude than for *H/D=1* at *r/D=4,* they act over a smaller area. Increasing the jet spacing from *H/D=1* to *H/D=1.5* increases $\bar{h}$ by *11%*; this increase occurs even though the arrival velocity is likely to be reduced. This is therefore attributed to the secondary peaks in heat transfer which are of the same magnitude as at *H/D=1* but act over a much larger area. At nozzle to impingement surface spacings greater than *1.5D*, the area averaged heat transfer remains fairly constant while stagnation region heat transfer is reducing this is due to the jet spreading at higher H/D and acting over a larger area.
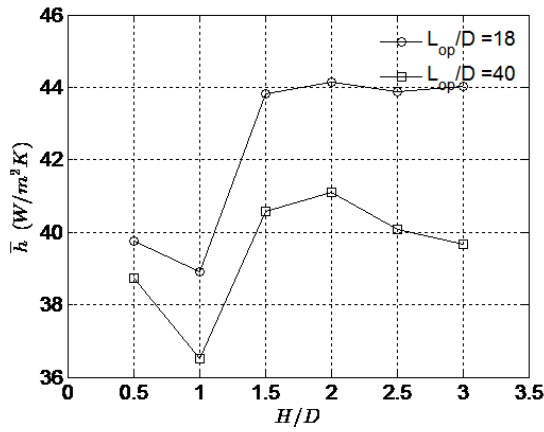
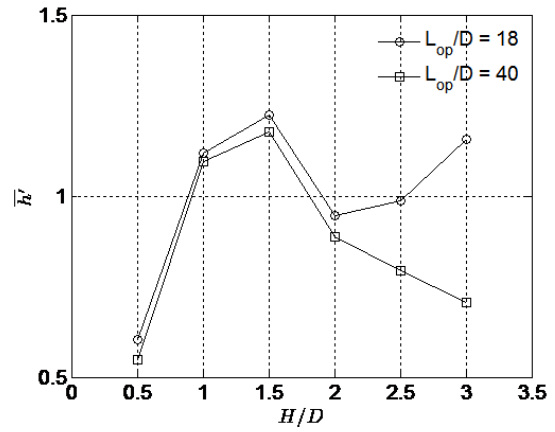Figure 9: $\bar{h}$ for semi-confined jet at *Re=3000 L_0/D=15*

Figure 10: $\bar{h'}$ for semi-confined jets *Re=3000 L_0/D=15*

By comparing the trends for *L_{op}/D=18* and *L_{op}/D=40* in figure 9, it can be seen that the increase in length of the confining plate has reduced the level of area averaged heat transferred to the jet across the full range of *H/D* tested. It is also evident that after both jets reached their maximum $\bar{h}$ at *H/D=2* heat transfer to the *L_{op}/D=40* jet is reduced more significantly with increasing *H/D* than for *L_{op}/D=18*. Figure 10 shows the area averaged fluctuations in heat transfer for the same range of parameters. It can be seen that the level of fluctuations remain similar for *H/D≤2*; for larger values of H/D the trends diverge and at *H/D=3* the fluctuations in heat transfer for *L_{op}/D=18* are double those of *L_{op}/D=40*. Again, as with stagnation region heat transfer, it is clear that the reduced levels of area averaged heat transfer observed for *L_{op}/D=40* at *H/D≥2* can be associated with the low levels of fluctuations when compared with less confined jet.

It has been shown that confinement of impinging synthetic jets has a significant impact on the cooling performance. While the reduction in performance caused by proximity to the heated surface can be overcome by operating the jet at higher H/D, this may not always be practical. The loss of efficiency caused by the addition of a longer orifice plate becomes more significant with increasing H/D; this is unique to synthetic jets in that the confinement effect in steady jets is less significant with increasing H/D.

3.3 EFFECT OF DUCTING ON THE HEAT TRANSFER RATE OF A SYNTHETIC AIR JET

In order to improve the performance of impinging synthetic jets in confined situations, a duct is attached to the base of the jet with a clearance of *1.5mm* which can be seen on figure 1. This is to enable ambient air from some remote location to be entrained during the suction phase of the cycle into the jet flow and to reduce the interactions between the expelled jet and arriving air. Three different duct outlet diameters were employed in this investigation (*6, 8* and *10mm*), equivalent to *1.2, 1.8* and *2* jet diameters.

The performance of the three configurations of ducting where compared with an un-ducted jet at *H/D=1* to 3. When comparing ducted and un-ducted jets the absolute height of the jet orifice above the foil is used as opposed to the height of the ducting above the foil. The addition of ducting plates increases the confinement of the jet to *L_{op}/D=40*, therefore the performance of the ducted jet is compared to that of a similarly confined un-ducted jet.

The stagnation region heat transfer to the three configurations of ducted jets compared with an un-ducted jet is presented in figure 11. Across the range of *H/D* tested all of the ducting configurations outperform the un-ducted jet. For all ducting configurations heat transfer is a maximum at *H/D=1* which indicates that ducting successfully negates the effects of confinement due to low *H/D* allowing the jet to deliver maximum heat transfer when the arrival velocity of the jet is highest. The *1.6 D* outlet duct performs best across the range of *H/D* tested delivering the highest rates of heat transfer at all jet spacings except *H/D=1* where the *2 D* outlet duct offers the greatest increase.
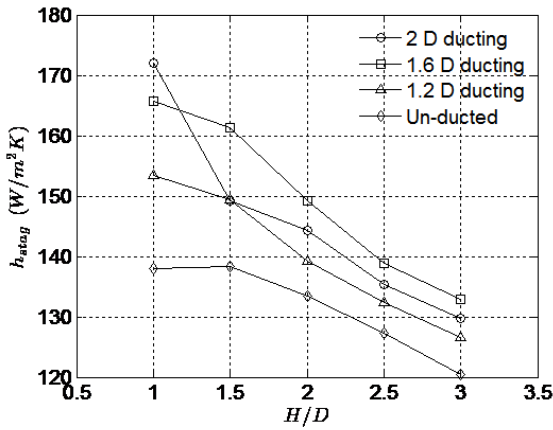
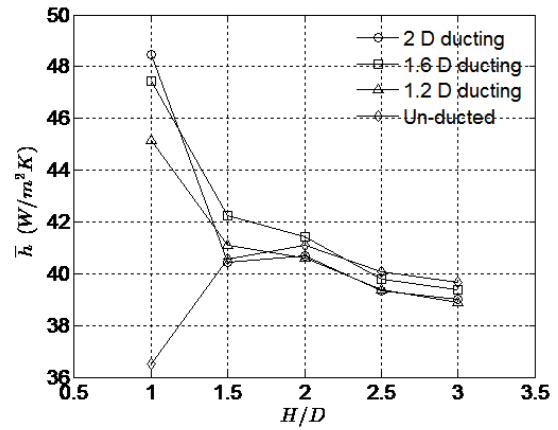Figure 11: Un-ducted and ducted configurations h_{stag};
Re=3000, L0/D=15

Figure 12: Un-ducted and ducted $\bar{h}$; Re=3000; $L_0/D=15$

Figure 12 shows the area averaged heat transfer corresponding to the three configurations of ducted jets compared with an un-ducted jet. Again the *1.8D* ducting performs best across the range of spacings tested and performs better than the un-ducted jet across the range of *H/D* but the *2D* ducting offers a higher increase in heat transfer at *H/D=1.* Comparing figures 11 and 12 it can been seen that ducting is more effective across the range of *H/D* in the stagnation region than it is for the area averaged heat transfer. It is also apparent that at *H/D=1* ducting offers a greater increase in heat transfer on an area averaged basis than in the stagnation region.
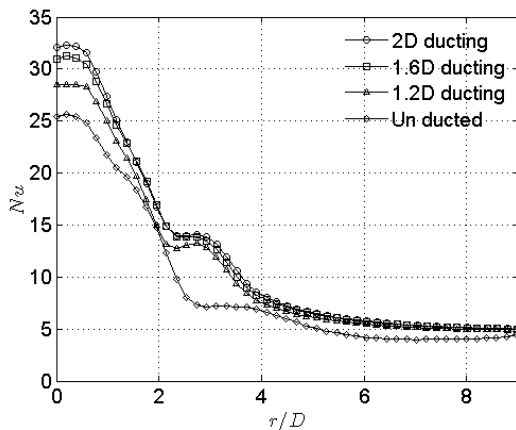

Figure 13: un-ducted and ducted *Nu* distributions
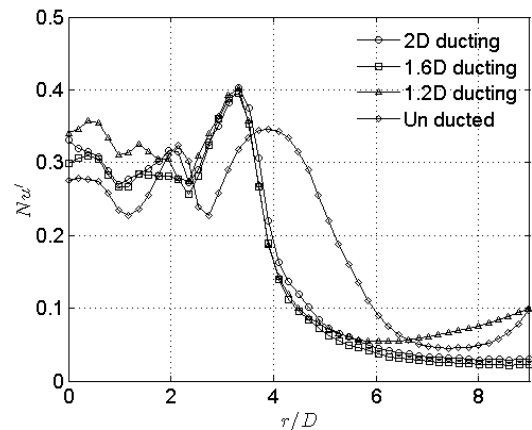*H/D=1 Re=3000 L0/D=15*

Figure 14: un-ducted and ducted *Nu'* distributions
H/D=1 Re=3000 L0/D=15

Figure 13 shows the heat transfer distribution for an un-ducted and ducted jet at *H/D=1*. It can be seen that the addition of ducting has moved the peaks in heat transfer which have been shown by O'Donovan and Murray [24, 25] to be associated with the breakdown of vortices in the wall jet closer to the centre of impingement as well as increasing the stagnation point heat transfer when compared to un-ducted jet. It is also noticeable that a change in the slope of the heat transfer distribution which is apparent for the un-ducted jet at *r/D≈1.5* is not present in the ducted jets.

Figure 14 shows the distributions of the fluctuations in heat transfer corresponding to figure 13. By comparing the profiles presented in figures 13 and 14 it can be seen that the *1.2D* ducting has comparatively high levels of stagnation region fluctuations but this results in a lower rate of surface heat transfer than the *1.6* and *2* jet diameter outlet ducting cases. This is attributed to the ducting outlet interacting with the exiting jet flow and increasing the turbulence in the flow but not the entrainment. The peak in the mean heat transfer at *r/D≈3* is lower than that observed for the larger ducting outlets but is a much sharper change in the rate of heat transfer while the peak in the fluctuations visible at the same radial location in figure 14 is the same for all three ducting configurations.

The level of heat transfer fluctuations for the *1.6D* outlet is lower than for the *1.2D* outlet but the stagnation region heat transfer is higher. Comparing the magnitude of the fluctuations in figure 14 at *r/D=2* for the *1.6D* outlet ducting and the un-ducted jet it is clear that the un-ducted jet has much higher fluctuations at this point; the fluctuations in the region where shown previously to be caused by the interactions between the two jet flow regimes. The low stagnation region *Nu'* and lack of interactions at *r/D=2* suggest that *1.6 D* outlet ducting does not restrict the exiting jet but reduces the interactions between the two flow regimes. This, in turn, reduces recirculation of heated air and increases heat transfer due to the entrainment of cooler ambient air.

By comparing the level of fluctuations in heat transfer for the *2D* outlet and the *1.6D* outlet, it is clear that there is little difference in their profile across the surface of the foil except at *r/D=2* where Nu' is higher in the case of the *2D* outlet duct than both the *1.2* and *1.6 D* outlet. No corresponding change in the rate of heat transfer is evident in figure 13 but the *2 D* ducting does give the highest heat transfer in both the stagnation region and on an area averaged basis.

4 CONCLUSIONS

Heat transfer to confined, un-ducted and ducted synthetic air jets has been investigated experimentally. Heat transfer to the jet is reported for a range of experimental parameters including jet exit to impingement surface spacings *H/D* (*0.5* to *3* jet diameters), at a Reynolds number, *Re=3000* with a non-dimensional Stroke length, *L_{0/D}=15*. A range of ducting outlet sizes were also investigated (*1.2*, *1.6* and *2* jet diameters).

Increasing confinement of the jet was shown to reduce the cooling performance of the jet by up to *14%* in the stagnation region and *8%* on an area averaged basis. Ducting was added to enable ambient air from a remote location to be entrained during the suction phase of the cycle into the jet flow and to reduce the interactions between the expelled jet and arriving air. This was shown to be an effective way to counteract the effects of both semi-confinement and confinement. Across the range of jet to impingement surface spacings tested ducting offered the largest increase in heat transfer at *H/D=1*; at this spacing the *2* jet diameter ducting outperforms all others and can increase the heat transferred to the jet in the stagnation region by 27% and on an area average basis by *36%.* At all other spacings ducting with a *1.6* jet diameters outlet offers the largest increase in heat transfer.

NOMENCLATURE

D	Jet diameter, *m*	q	Rate of heat transfer, *W*
f_e	Excitation frequency, *Hz*	r	Distance from geometric centre, *m*
H	Height of nozzle above surface, *m*	Re	Reynolds number, $\rho UD /\mu$
k	Thermal conductivity, *W/mK*	St	Strouhal number, *fD/U*
L_0	Jet stroke length, *m*	T	Temperature °*K*
L_{op}	Orifice plate length, *m*	U_0	Jet velocity, *m/s*
Nu	Nusselt number	V	Voltage, *V*
Nu'	root-mean-square Nusselt number	Greek letters	
$\overline{Nu}$	Area-averaged Nusselt number	ν	Kinematic viscosity, m^2/s
Nu_{stag}	Stagnation region Nusselt number	ρ	Density, kg/m^3
p	Pressure, *Pa*	τ	½ cycle period, expulsion stroke, *s*

REFERENCES

1.   Hoefler, F., et al., *Heat Transfer Characteristics of an Oblique Jet Impingement Configuration in a Passage With Ribbed Surfaces.* Journal of Turbomachinery, 2012. **134**(3): p. 031022.

2. O'Donovan, T.S., D.B. Murray, and A.A. Torrance, *Jet heat transfer in the vicinity of a rotating grinding wheel.* Proceedings of the Institution of Mechanical Engineers Part C - Journal of Mechanical Engineering Science, 2006. **220**(6): p. 837-845.

3. Garimella, S.V. and V.P. Schroeder, *Local heat transfer distributions in confined multiple air jet impingement.* ASME Journal of Electronic Packaging, 2001. **123**: p. 165 - 172.

4. Smith, B.L. and G.W. Swift, *A comparison between synthetic jets and continuous jets.* Experiments in Fluids, 2003. **34**: p. 467 - 472.

5. Pavlova, A. and M. Amitay, *Electronic cooling using synthetic jet impingement.* ASME Journal of Heat Transfer, 2006. **128**: p. 897 - 907.

6. Kercher, D.S., et al., *Microjet cooling devices for thermal management of electronics.* IEEE Transactions on Components and Packaging Technologies, 2003. **26**: p. 359 - 366.

7. Saini, M. and R.L. Webb, *Heat rejection limits of air cooled plane fin heat sinks for computer cooling.* IEEE Transactions on Components and Packaging Technologies, 2003. **26**(1): p. 71-79.

8. S. Gunther, F.B., D. M. Carmean, J. C. Hall, *Managing the Impact of Increasing Microprocessor Power Consumption* Intel Technology Journal, 2001. **Vol. 5,** (No. 1).

9. Holman, R., et al., *Formation criterion for synthetic jets.* AIAA Journal, 2005. **43**: p. 2110 - 2116.

10. Smith, B.L. and A. Glezer, *The formation and evolution of synthetic jets.* Physics of Fluids, 1998. **10**: p. 2281 - 2297.

11. Persoons, T. and T.S. O'Donovan, *A pressure-based estimate of synthetic jet velocity.* Physics of Fluids, 2007. **19**.

12. Chaudhari, M., B. Puranik, and A. Agrawal, *Heat transfer characteristics of synthetic jet impingement cooling.* International Journal of Heat and Mass Transfer, 2010. **53**(5–6): p. 1057-1069.

13. Persoons, T., A. McGuinn, and D.B. Murray, *A general correlation for the stagnation point Nusselt number of an axisymmetric impinging synthetic jet.* International Journal of Heat and Mass Transfer, 2011. **54**(17–18): p. 3900-3908.

14. Ashforth-Frost, S. and K. Jambunathan, *Effect of nozzle geometry and semi-confinement on the potential core of a turbulent axisymmetric free jet.* International Communications in Heat and Mass Transfer, 1996. **23**: p. 155 - 162.

15. Garimella, S.V. and R.A. Rice, *Confined and submerged liquid jet impingement heat transfer.* ASME Journal of Heat Transfer, 1995. **117**: p. 871 - 877.

16. Colucci, D.W. and R. Viskanta, *Effect of nozzle geometry on local convective heat transfer to a confined impinging air jet.* Experimental Thermal and Fluid Science, 1996. **13**: p. 71 - 80.

17. Gao, N. and D. Ewing, *Investigation of the effect of confinement on the heat transfer to round impinging jets exiting a long pipe.* International Journal of Heat and Fluid Flow, 2006. **27**(1): p. 33-41.

18. Youn, Y.J., K. Choo, and S.J. Kim, *Effect of confinement on heat transfer characteristics of a microscale impinging jet.* International Journal of Heat and Mass Transfer, 2011. **54**(1-3): p. 366-373.

19. Persoons, T. and T.S. O'Donovan, *High Dynamic Velocity Range Particle Image Velocimetry Using Multiple Pulse Separation Imaging.* Sensors, 2010. **11**(1): p. 1-18.

20. Patil, V.A. and V. Narayanan, *Application of heated-thin-foil thermography technique to external convective microscale flows.* Measurement Science and Technology, 2005. **16**: p. 472-476.

21. Golobic, I., et al., *Experimental determination of transient wall temperature distributions close to growing vapor bubbles.* Heat and Mass Transfer, 2009. **45**(7): p. 857-866.

22. Beranek, L.L., *Acoustics* 1993: Acoustical Society of America, Melville, NY. p 133.

23. Gardon, R.J. and J.C. Akfirat, *The role of turbulence in determining the heat transfer characteristics of impinging jets.* International Journal of Heat and Mass Transfer, 1965. **8**: p. 1261 - 1272.

24. O'Donovan, T.S. and D.B. Murray, *Jet impingement heat transfer - Part I: Mean and root-mean-square heat transfer and velocity distributions.* International Journal of Heat and Mass Transfer, 2007. **50**(17-18): p. 3291-3301.

25. O'Donovan, T.S. and D.B. Murray, *Jet impingement heat transfer - Part II: A temporal investigation of heat transfer and local fluid velocities.* International Journal of Heat and Mass Transfer, 2007. **50**(17-18): p. 3302-3314.